

## The OATMEAL Survey. II. The 3D spin-orbit obliquity of an eccentric transiting brown dwarf in the Ruprecht 147 open cluster

Theron W. Carmichael,<sup>1,\*</sup> Steven Giacalone,<sup>2,†</sup> Noah Vowell,<sup>3,4</sup> Daniel Huber,<sup>1</sup> Xian-Yu Wang,<sup>5</sup>  
Malik Bossett,<sup>6</sup> Luke Handley,<sup>2</sup> Aaron Householder,<sup>7,8</sup> Yaguang Li,<sup>1</sup> Benjamin J. Fulton,<sup>9,10</sup>  
Andrew Howard,<sup>9</sup> Howard Isaacson,<sup>11</sup> Samuel Halverson,<sup>12</sup> and Arpita Roy<sup>13</sup>

<sup>1</sup>*Institute for Astronomy, University of Hawai'i, 2680 Woodlawn Drive, Honolulu, HI 96822, USA*

<sup>2</sup>*Department of Astronomy, California Institute of Technology, Pasadena, CA 91125, USA*

<sup>3</sup>*Center for Data Intensive and Time Domain Astronomy, Department of Physics and Astronomy, Michigan State University, East Lansing, MI 48824, USA*

<sup>4</sup>*Center for Astrophysics | Harvard & Smithsonian, 60 Garden St, Cambridge, MA 02138, USA*

<sup>5</sup>*Department of Astronomy, Indiana University, 727 East 3rd Street, Bloomington, IN 47405, USA*

<sup>6</sup>*Department of Astronomy and Astrophysics, University of California, Santa Cruz, CA 95064, USA*

<sup>7</sup>*Department of Earth, Atmospheric and Planetary Sciences, Massachusetts Institute of Technology, Cambridge, MA 02139, USA*

<sup>8</sup>*Kavli Institute for Astrophysics and Space Research, Massachusetts Institute of Technology, Cambridge, MA 02139, USA*

<sup>9</sup>*Cahill Center for Astronomy & Astrophysics, California Institute of Technology, Pasadena, CA 91125, USA*

<sup>10</sup>*IPAC-NASA Exoplanet Science Institute, Pasadena, CA 91125, USA*

<sup>11</sup>*Department of Astronomy, University of California Berkeley, Berkeley, CA 94720, USA*

<sup>12</sup>*Jet Propulsion Laboratory, California Institute of Technology, 4800 Oak Grove Drive, Pasadena, CA 91109, USA*

<sup>13</sup>*Astrophysics & Space Institute, Schmidt Sciences, New York, NY 10011, USA*

### ABSTRACT

We present new analysis of the CWW 89 system as part of the Orbital Architectures of Transiting Massive Exoplanets And Low-mass stars (OATMEAL) survey. The CWW 89 system is a member of the 2.8 Gyr old Ruprecht 147 (NGC 6774) cluster and features two stars, CWW 89A (EPIC 219388192) and CWW 89B, with the primary hosting a transiting brown dwarf. We use in-transit, highly precise radial velocity measurements with the Keck Planet Finder (KPF) to characterize the Rossiter-McLaughlin (RM) effect and measure the projected spin-orbit obliquity  $|\lambda| = 1.4 \pm 2.5^\circ$  and the full 3D spin-orbit obliquity of the brown dwarf to be  $\psi = 15.1^{+15.0}_{-10.9}$ . This value of  $\lambda$  implies that the brown dwarf's orbit is prograde and well-aligned with the equator of the host star, continuing the trend of transiting brown dwarfs showing a preference for alignment ( $\lambda \approx 0^\circ$ ) regardless of the stellar effective temperature. We find that this contrast with the transiting giant planet population, whose spin-orbit alignments depend on host  $T_{\text{eff}}$ , shows an increasingly clear distinction in the formation and orbital migration mechanisms between transiting giant planets and transiting brown dwarfs like CWW 89Ab. For this system in particular, we find it plausible that the brown dwarf may have undergone coplanar high-eccentricity migration influence by CWW 89B.

**Keywords:** Brown dwarfs (185) — Exoplanet dynamics (490) — Exoplanet migration (2205) — Star-planet interactions (2177)

### 1. INTRODUCTION

Our understanding of the tidal realignment of close-in planetary orbits around main sequence stars has sub-

stantially improved since the first measurements of spin-orbit obliquities were made for gas giant planets (D. Queloz et al. 2000a; J. N. Winn et al. 2005; A. H. M. J. Triaud et al. 2010; T. Hirano et al. 2011; S. Albrecht et al. 2012). Here, we define “spin-orbit obliquity” to mean the angle between the rotation axis of the primary star and the orbital axis of the companion(s). With recent works by J. Zak et al. (2024); J. I. Espinoza-Retamal et al. (2024); E. Knudstrup et al. (2024); X.-Y.

Corresponding author: Theron W. Carmichael  
tcarmich@hawaii.edu

\* NSF Ascend Fellow

† NSF Astronomy and Astrophysics Postdoctoral Fellow

Wang et al. (2024); J. Zhang et al. (2025), the number of obliquity measurements made for giant planets now numbers in the dozens, with a wide range of aligned to misaligned systems. A relatively coherent story is emerging for the orbital evolution of these systems and it is centered on a general theory of the interior structures of stars that host giant planets. As main sequence stars that are more massive than the Sun evolve, expand in radius, and decrease in effective temperature, their outer envelopes transition from being predominantly radiative to convective. R. P. Kraft (1967) first established a temperature threshold at which this change occurs, now known as the Kraft Break ( $T_{\text{eff}} = 6250\text{K}$ ). From this, a trend in the projected spin-orbit alignments, or obliquities  $\lambda$ , for giant planets around the Kraft Break has emerged: Stars hotter than the Kraft Break show a population of planets with no preferential value of  $\lambda$  whereas stars cooler than the Kraft Break yield a companion planet population with preferentially aligned obliquities ( $\lambda = 0^\circ$ ) (e.g. J. N. Winn et al. 2010; M. Rice et al. 2022; J. Ruzsna et al. 2024). Recent observations of subgiant stars that have crossed the Kraft break during their evolution confirmed that alignments of giant planets are strongly tied to presence of convective envelopes (e.g. N. Saunders et al. 2024).

The more massive siblings to giant planets, brown dwarfs (BDs), have recently seen a boom in their known transiting population in large part thanks to the TESS mission (G. R. Ricker et al. 2015) and efforts from ground-based facilities like the Next Generation Transit Survey (NGTS) (P. J. Wheatley et al. 2018). Recent works from (B. A. Henderson et al. 2024a; N. Vowell et al. 2025; A. Larsen et al. 2025, and references therein) show more than 50 known transiting brown dwarfs and like with their giant planet siblings, astronomers have pursued measurements of their spin-orbit obliquities for insight into their orbital histories. However, in contrast to the dozens spin-orbit alignments measured for transiting giant planets, only 9 such measurements exist for transiting BDs. Every measurement of  $\lambda$  for transiting BDs thus far indicates a preference for an aligned orbit (A. H. M. J. Triaud et al. 2009; R. J. Siverd et al. 2012; A. H. M. J. Triaud et al. 2013; G. Zhou et al. 2019; S. Giacalone et al. 2024; T. Ferreira dos Santos et al. 2024; M. Brady et al. 2025; L. Doyle et al. 2025; C. M. Johns-Krull et al. 2008).

One widely-used technique to measure  $\lambda$  for transiting system is the Rossiter-McLaughlin (RM) Effect (D. Queloz et al. 2000b; A. H. M. J. Triaud 2018). This requires taking spectra of the host star during a transit to observe the radial velocity (RV) anomaly induced by the transiting companion blocking varying amounts of red-

or blue-shifted light depending on the orbital configuration relative to the orientation of the host star’s spin axis. The RM effect alone can only offer an estimate of the *projected* spin-orbit alignment  $\lambda$ , but in some cases, the system supplies all of the ingredients needed to determine the full 3D obliquity  $\psi$ , namely both the orbital inclination of the transiting companion and the stellar spin axis angle, which is determined from combining the projected rotational velocity of the star with its rotation period (often observed via photometric modulations in its light curve).

Here we present an RM measurement of  $\lambda$  for the transiting BD CWW 89Ab. CWW 89Ab’s environment distinguishes it from other BD systems with measured obliquities. The CWW 89 system receives its name from J. L. Curtis et al. (2013a), who catalog it and over 100 other stars as members of the Ruprecht 147 open cluster. This makes CWW 89Ab one of four known transiting BDs that reside in a stellar association or cluster (the other three being AD 3116b in Praesepe, RIK 72b in Upper Scorpius, and HIP 330609b in MELANGE 6 from E. Gillen et al. (2017), T. J. David et al. (2019), and N. Vowell et al. (2023) respectively), and the oldest BD to reside in such an environment at  $2.76 \pm 0.61$  Gyr (G. Torres et al. 2018). CWW 89 consists of a primary G-dwarf star, CWW 89A, and a secondary M-dwarf, CWW 89B, orbiting at a 24.9 AU (81 mas) projected separation (T. G. Beatty et al. 2018). A handful of transiting BD systems comprise 3 or more objects, typically a primary star, a transiting BD companion, and a more distant outer stellar companion, but CWW 89 is the only multi-star transiting BD system featuring a G-dwarf star as its primary.

The paper proceeds as follows: Section 2 details past and new RV measurements used in the orbital solution and characterization of the RM effect, respectively. Section 3 details our RM model, calculation of the stellar spin axis angle, and the determination of the full 3D obliquity. Section 4 outlines considerations for the emerging trend in spin-orbit alignments for the transiting brown dwarf population.

## 2. OBSERVATIONS

### 2.1. Keck Planet Finder in-transit RVs

From 07:10 UT to 12:19 UT on 2024 July 30, we observed a transit of the CWW 89Ab using the Keck Planet Finder (KPF; S. R. Gibson et al. 2024a) with the Keck I telescope at the W. M. Keck Observatory located on Maunakea, HI, USA. To ensure sufficient pre- and post-transit baseline, we observed the star continuously from approximately 1 hour before ingress to 1 hour after egress. We took a series of spectra with KPF

at 600 s exposure times each, resulting in 20 in-transit observations at a SNR of 60-90 across the 500-600 nm wavelength range. The goal was to maintain a SNR at this level or higher while keeping good coverage of the transit so that the RV anomaly induced by the RM effect would be well-characterized. The RVs are calculated using the KPF data reduction pipeline (S. R. Gibson et al. 2024b). The complete series of KPF RVs are given in Table 1. We note that KPF produces RVs in a green and red CCD, taking the RV values from different orders in the echelle spectrum.

Based on reported the stellar parameters in G. Nowak et al. (2017) and T. W. Carmichael et al. (2019) of  $M_\star = 1.1 M_\odot$ ,  $R_\star = 1.0 R_\odot$ ,  $T_{\text{eff}} = 5755 \text{ K}$ ,  $\log g = 4.5$ , and  $[\text{Fe}/\text{H}] = 0.2$ , we assume CWW 89A is a sunlike star. We only use the RVs derived from the green CCD as these are at a higher SNR than those of the red CCD for this star by a factor of  $\lesssim 2.5$ .

### 2.2. Literature RVs from TRES and FIES

Past works by G. Nowak et al. (2017) and T. W. Carmichael et al. (2019) have published orbital solutions (i.e. out-of-transit spectra) for CWW 89A. These data are used to remove the Keplerian motion from the in-transit RVs newly collected with KPF. These data aid in the detailed analysis of the RM effect to account for the out-of-transit motion of the brown dwarf.

T. W. Carmichael et al. (2019) provide 18 RVs measured from spectra taken with the Tillinghast Reflector Echelle Spectrograph (TRES) located at the Fred Lawrence Whipple Observatory at Mt. Hopkins, AZ, USA. These data were acquired from 2015 September 24 to 2016 May 30. Here, we simply use the values published in Table 2 of T. W. Carmichael et al. (2019).

G. Nowak et al. (2017) provide 9 RVs measured from spectra acquired with the Fiber-fed Echelle Spectrograph (FIES) from 2016 May 15 to 2016 June 29. FIES is located at Roque de los Muchachos Observatory in La Palma, Spain. G. Nowak et al. (2017) also publish 3 RV measurements from the Tull Coude Spectrograph, but we omit these from the present work as these data showed significantly more scatter than the FIES or the TRES data (a few hundred  $\text{m s}^{-1}$  from Tull compared to  $< 50 \text{ m s}^{-1}$  for TRES and FIES).

### 2.3. K2 Data

We use photometric time series from the K2 missions as part of our joint modeling of the RM effect. The K2 data are acquired from the Mikulski Archive for Space Telescopes and are processed following the methods outlined in T. W. Carmichael et al. (2019). We note that TESS is scheduled to observe CWW 89A in its sector

**Table 1.** In-transit KPF relative RV time series for CWW 89A. We subtract the mean of the RVs ( $47262 \text{ m s}^{-1}$ ) arbitrarily for the purpose of displaying the data in this table.

BJD <sub>TDB</sub>	RV - 47250 ( $\text{m s}^{-1}$ )	$\sigma_{\text{RV}}$ ( $\text{m s}^{-1}$ )
2460521.8046937	526.92	4.28
2460521.8119592	489.96	4.42
2460521.8198269	446.04	5.19
2460521.8267481	412.76	4.81
2460521.8355091	361.17	4.67
2460521.8415548	341.3	6.27
2460521.8503282	304.77	4.4
2460521.8575215	284.0	3.55
2460521.8646204	243.27	5.09
2460521.8725758	209.82	4.2
2460521.8799776	168.5	3.79
2460521.8876566	130.2	4.21
2460521.8963321	79.69	4.89
2460521.9031678	38.74	3.77
2460521.9108818	-6.41	3.88
2460521.9181893	-50.28	3.62
2460521.9252793	-90.72	3.99
2460521.9333313	-133.15	4.36
2460521.9405187	-175.64	4.66
2460521.948442	-210.8	4.58
2460521.9559914	-253.12	4.18
2460521.9633564	-281.51	4.15
2460521.9709421	-308.74	4.16
2460521.9782791	-328.87	4.04
2460521.9859417	-365.23	3.94
2460521.993371	-403.39	4.12
2460522.0004741	-436.12	4.69
2460522.0083231	-479.83	6.05
2460522.0161146	-513.33	5.3

92 (May 2025) of Extended Mission 2, so those data are not include here.

## 3. ANALYSIS

We jointly model the KPF, TRES, and FIES RVs, K2 light curves, and host star broadband SED photometry using a modified version<sup>14</sup> of EXOFASTv2 (J. D. Eastman et al. 2019) where instead of using a simplified approximation for the RM effect from, Y. Ohta et al. (2005), we employ a more robust calculation from T. Hirano et al. (2011), which accounts for several subtle effects, including stellar rotation, macroturbulence, thermal broadening, pressure broadening, and instrumental broadening.

<sup>14</sup> Modified EXOFASTv2

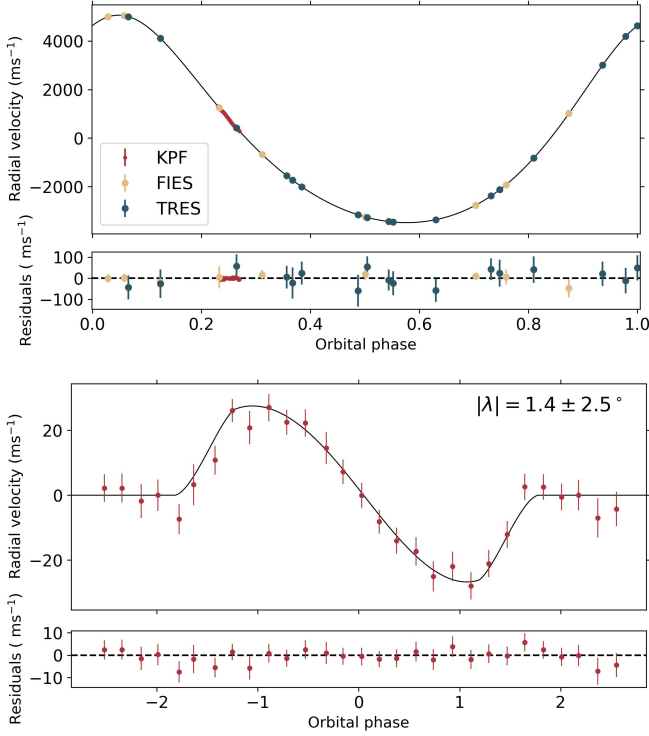


**Figure 1.** *Top:* RV orbital solution for CWW 89A using TRES (T. W. Carmichael et al. 2019) and FIES (G. Nowak et al. 2017) data. *Bottom:* KPF in-transit RV data showing the RV anomaly induced by the Rossiter-McLaughlin Effect.

We set either uniform  $\mathcal{U}[a, b]$  or Gaussian  $\mathcal{G}[a, b]$  priors on our input parameters (see Table 3). These priors have mean values  $a$  with width values  $b$ . We use spectroscopic priors on  $T_{\text{eff}}$  and  $[\text{Fe}/\text{H}]$  from T. W. Carmichael et al. (2019), zero-point corrected (L. Lindegren et al. 2018) parallax priors from Gaia DR3, and an upper limit on V-band extinction ( $A_V$ , E. F. Schlafly & D. P. Finkbeiner 2011). J. L. Curtis et al. (2013b) confirm the CWW 89 system to be a probable member of the Ruprecht 147 open cluster, so we additionally set the cluster’s age of  $2.76 \pm 0.61$  (G. Torres et al. 2018) as a prior. We let the RV offsets  $\gamma$  for each instrument be free parameters and we include an RV jitter term,  $\sigma_j$ , for each RV dataset to account for the surface activity of the star. The RV jitter term is based on a white noise model implemented in EXOFASTv2. We use values from T. W. Carmichael et al. (2019) for the following parameters to set as starting points for our fit: the orbital period, mid-transit time, orbital inclination, and the companion-to-host radius ratio.

For the RM model, we model the limb-darkening for KPF assuming a  $V$  bandpass wavelength range. We fix  $v_\alpha$  to 0 (ignore differential rotation) and we use scaling relations for  $v_\zeta$  (macroturbulence) from A. P.

**Table 2.** Table of transiting brown dwarf projected obliquities  $\lambda$  and 3D obliquities  $\psi$ . Values for CWW 89Ab are from this work.

Object	Mass ( $M_J$ )	$ \lambda $ (degrees)	$\psi$ (degrees)	Source
HATS-70b	$12.9 \pm 1.8$	$8.9 \pm 5.6$	-	1
GPX-1b	$19.7 \pm 1.6$	$6.9 \pm 10.0$	-	2
CoRoT-3b	$22.3 \pm 1.0$	$37.6^{+10.0}_{-22.3}$	-	3
KELT-1b	$27.3 \pm 0.5$	$2.0 \pm 16$	-	4
CWW 89Ab	$39.2 \pm 1.1$	$1.4 \pm 2.5$	$15.1^{+15.0}_{-10.9}$	-
WASP-30b	$62.5 \pm 1.2$	$7.0^{+19.0}_{-27.0}$	-	5
TOI-2119b	$64.4 \pm 5.3$	$0.8 \pm 1.1$	$15.7 \pm 5.6$	6
LP 261-75C	$67.4 \pm 2.1$	$4.8^{+11.3}_{-10.2}$	$14.0^{+7.8}_{-6.7}$	7
TOI-2533b	$74.9 \pm 5.3$	$7.0 \pm 14.0$	-	8

References: 1) G. Zhou et al. (2019), 2) S. Giacalone et al. (2024), 3) A. H. M. J. Triaud et al. (2009), 4) R. J. Siverd et al. (2012), 5) A. H. M. J. Triaud et al. (2013), 6) L. Doyle et al. (2025), 7) M. Brady et al. (2025), 8) T. Ferreira dos Santos et al. (2024)

Doyle et al. (2014) and for  $v_\xi$  (microturbulence) from H. Bruntt et al. (2010). Both  $v_\zeta$  and  $v_\xi$  have uniform priors. From this joint analysis of the stellar properties, transit photometry, and RVs, we find a projected obliquity angle of  $|\lambda| = 1.4 \pm 2.5^\circ$  for CWW 89Ab.

All stellar parameters we derive are consistent within  $< 2\sigma$  of those determined in G. Nowak et al. (2017) and T. W. Carmichael et al. (2019). Our full list of derived parameters are shown in Table 3. We highlight our derived  $T_{\text{eff}} = 5680 \pm 86\text{K}$  for CWW 89A as this is especially relevant in our discussion of the realignment timescale for CWW 89Ab. A summary of other basic parameters we derive:  $M_\star = 1.02 \pm 0.03 M_\odot$ ,  $R_\star = 1.07 \pm 0.02 R_\odot$ ,  $[\text{Fe}/\text{H}] = 0.07 \pm 0.09$ ,  $M_b = 37.3 \pm 1.6 M_J$ ,  $R_b = 0.96 \pm 0.04 R_J$ ,  $P_{\text{orb}} = 5.29$  days.

### 3.1. The 3D spin-orbit obliquity

With our newly measured projected obliquity in hand, we may determine the 3D spin-orbit obliquity of the system. This is the angle between the spin axis of the primary star and the orbital axis of the brown dwarf companion. by combining  $\lambda$  with the stellar spin axis inclination angle,  $i_\star$ , and the orbital inclination angle of the BD,  $i_0$ . The 3D obliquity may be calculated via:

$$\cos \psi = \cos i_\star \cos i_0 + \sin i_\star \sin i_0 \cos \lambda \quad (1)$$

This form of the relationship between  $\psi$ ,  $\lambda$ ,  $i_\star$ , and  $i_0$  follow from S. H. Albrecht et al. (2022). The first report of the rotation period of CWW 89A comes from G. Nowak et al. (2017) on an analysis of the  $K2$  light curve showing a  $P_{\text{rot}} = 12.6 \pm 2.1$  days. If we adopt this value and the  $v \sin i_\star = 4.1 \pm 0.4 (1.0) \text{ km s}^{-1}$  from



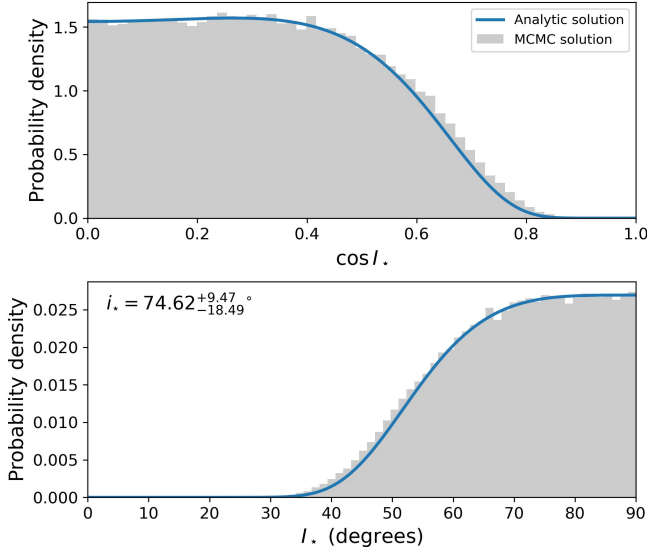


**Figure 2.** The posterior distribution for the stellar inclination angle  $i_*$  for CWW 89A. We use the  $P_{\text{rot}}$  measured from G. Nowak et al. (2017) and the sampling method first presented in K. Masuda & J. N. Winn (2020) and described in B. P. Bowler et al. (2023) to derive an  $i_* = 74.7^{+9.4}_{-18.6}$ . We interpret this as aligned with the orbital inclination  $i_0$ .

G. Nowak et al. (2017), we may derive the stellar inclination as  $i_* = 74.7^{+9.4}_{-18.6}$  (Figure 2). The parenthetical uncertainty on  $v \sin i$  is the value we adopt given the typical challenges in small  $v \sin i$  measurements; our RM analysis also provides constraints on  $v \sin i$  (Table 3) and both  $v \sin i$  values are consistent with each other. This derivation follows that first outlined in K. Masuda & J. N. Winn (2020) and improved on in B. P. Bowler et al. (2023) using a bootstrap analysis of the relationship:

$$i_* = \sin^{-1} \left( \frac{v \sin i_*}{2\pi R_*/P_{\text{rot}}} \right) \quad (2)$$

Combining the results from this and Equation 1 yields a 3D obliquity value of  $\psi = 15.1^{+15.0}_{-10.9}$  for CWW 89Ab (Figure 3). This can be compared to  $\psi$  measured for other transiting BDs in Table 2, making CWW 89Ab the third transiting BD with a measurement of  $\psi$ .

#### 4. DISCUSSION

##### 4.1. The CWW 89 system

A collection of past studies (J. L. Curtis et al. 2013b; G. Torres et al. 2018; G. Nowak et al. 2017; T. G. Beatty et al. 2018; T. W. Carmichael et al. 2019) have helped construct a nearly-complete picture for the formation and evolution of the brown dwarf in the CWW 89 system. This section serves to contextualize the present work into this picture with the aim of further completing it with our new measurements of the orbital archi-

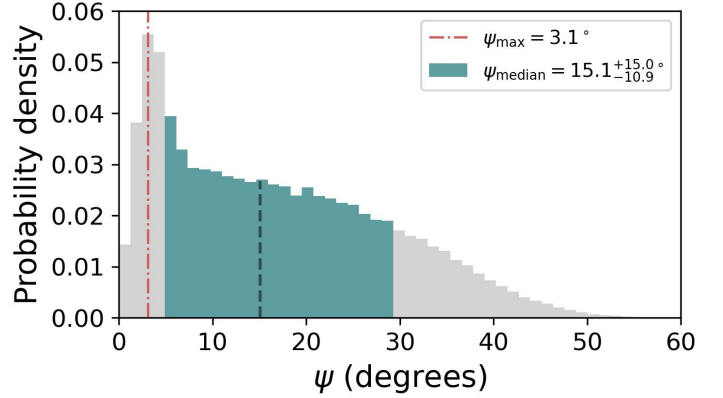


**Figure 3.** The posterior distribution of  $\psi$  from sampling in  $\cos \psi$  parameter space. Given the skewed nature of this distribution, a more conservative estimate of the 3D obliquity is  $\psi \leq 30.1^\circ$  with the peak of the distribution at  $\psi_{\text{peak}} = 3.1^\circ$ .

ture of CWW 89. Here are the following key features of the CWW 89 system:

- CWW 89A is a  $1.0 M_\odot$  star that hosts a distant  $0.5 M_\odot$  M-dwarf companion, CWW 89B, with a projected separation of 25 AU, or 81 mas, and  $\Delta K = 2.2$  dimmer than CWW 89A (T. G. Beatty et al. 2018)
- CWW 89 is a probable member of the Ruprecht 147 open cluster (J. L. Curtis et al. 2013b) with an age of  $2.76 \pm 0.61$  Gyr (G. Torres et al. 2018)
- The brown dwarf, CWW 89b, may have formed via core accretion given evidence presented in T. G. Beatty et al. (2018). In summary, secondary eclipses from *Spitzer*/IRAC (G. G. Fazio et al. 2004) indicate an over-luminous atmosphere of CWW 89Ab that is best explained by a temperature inversion caused by a superstellar C/O ratio in the brown dwarf. This favors a core accretion formation scenario.
- The tidal quality factor of CWW 89b is estimated to have a lower limit of  $Q_b \geq 10^{4.15}$  (T. G. Beatty et al. 2018), which yields a circularization timescale  $\tau_{\text{circ}} > 7.5$  Gyr (T. W. Carmichael et al. 2019)

Currently, it is unclear whether or not the secondary star, CWW 89B, is coplanar or not with CWW 89Ab—an especially important aspect to consider given the implications for the M-dwarf’s influence on the orbital evolution of the brown dwarf.

#### 4.2. Evidence for primordial alignment

Several factors affect the spin-orbit histories and outcomes for giant planet and brown dwarf companions to stars. Three key factors are: mass ratio  $q$ , scaled semi-major axis  $a/R_\star$ , and host star effective temperature. We show Figure 4 to illustrate the observed distribution in spin-orbit alignment  $\lambda$  as a function of  $T_{\text{eff}}$  or  $q$  (adapted from a similar figure in J. Rusznak et al. (2024)). These factors strongly dictate the circularization timescale  $\tau_{\text{circ}}$  and realignment timescale  $\tau_{\text{CE}}$  for giant planets and brown dwarfs, but importantly, these effects appear to be distinct between the two populations. From S. Albrecht et al. (2012), the realignment timescale is:

$$\tau_{\text{CE}} = 10 \times q^{-2} \left( \frac{a/R_\star}{40} \right)^6 \text{ Gyr} \quad (3)$$

for convective outer envelope (hence the CE subscript) stars  $T_{\text{eff}} \lesssim 6250\text{K}$ . We derive  $q = 0.036$  and  $a/R_\star = 12.608$  for CWW 89Ab.

From this, it follows that less-massive companions (smaller mass ratio  $q$ ) would have longer realignment timescales than more-massive companions around cool stars. The same conclusion is drawn for companions in larger scaled semi-major axis configurations. In the case of CWW 89A, Equation 3 indicates the realignment timescale is  $\tau_{\text{CE}} \approx 10$  Gyr, and greater than the  $2.76 \pm 0.61$  Gyr age of the system by  $>3\sigma$ . This implies that the spin-orbit alignment of the brown dwarf is primordial. On the contrary, when considering only the primary star, the provenance of the eccentricity of the brown dwarf is ambiguous given T. W. Carmichael et al. (2019) report the circularization timescale  $\tau_{\text{circ}} > 7.5$  Gyr using the tidal quality factor of  $Q_b \gtrsim 10^{4.15}$  for the brown dwarf from T. G. Beatty et al. (2018). This is again much longer than the system's age, but the fact that the eccentricity is  $e = 0.19$  means that this can be primordial or a result of interactions with the outer companion, CWW 89B. T. G. Beatty et al. (2018) report the  $Q_b$  based on an extrapolation using rotational angular momentum evolution calculations between a star and giant planet from J. Leconte et al. (2010). This calculation attempts to account for the exchange in energy via tides that result in the spin-up of the host star rotation rate and the increase in internal heat of the companion.

##### 4.2.1. Coplanar high-eccentricity migration

This brings us to one theory that could explain the non-zero eccentricity of CWW 89Ab while preserving a zero (aligned) spin-orbit angle. C. Petrovich (2015) present a framework that plausibly describes the story of CWW 89 via a *coplanar* high-eccentricity migration

(coplanar HEM) for the BD driven by the outer M-dwarf. In this scenario, a distant companion could be responsible for guiding the BD inwards to its current configuration should the following conditions be satisfied:

$$m_{\text{in}}/m_{\text{out}}(a_{\text{in}}/a_{\text{out}})^{1/2} \lesssim 0.16 \quad (4)$$

where  $m$  and  $a$  are the respective initial masses and semi-major axes of the inner (CWW 89Ab;  $a_{\text{in}} = 0.06$  AU,  $m_{\text{in}} = M_b = 39 M_J = 0.04 M_\odot$ ) and outer companion (CWW 89B;  $a_{\text{out}} \gtrsim 25$  AU,  $m_{\text{out}} = M_B = 0.5 M_\odot$ ). In the case of CWW 89, we are limited with a *projected* separation for CWW 89B, but even in the most conservative scenario (i.e. the minimum allowable  $a_{\text{out}}$ ) for this framework, the above inequality still holds, meaning that CWW 89B may have induced coplanar high-eccentricity migration of CWW 89Ab. This inequality assumes an initial eccentricity of the inner companion  $e \gtrsim 0.5$ , so we would require the eccentricity of the inner brown dwarf to sufficiently dampen from  $e \approx 0.5$  to  $e = 0.2$  for its present day configuration.

##### 4.2.2. Other massive hierarchical triple systems

There are 4 other transiting systems that feature an inner massive ( $\gtrsim 10 M_J$ ) companion with a measured spin-orbit angle and with confirmed or plausibly outer stellar companions. These are TOI-2119 (C. I. Cañas et al. 2022; T. W. Carmichael et al. 2022; L. Doyle et al. 2025), and TOI-2533 (S. P. Schmidt et al. 2023; T. Ferreira dos Santos et al. 2024), LP 261-75 (J. M. Irwin et al. 2018; M. Brady et al. 2025), and XO-3 (J. N. Winn et al. 2008; J. Rusznak et al. 2024). Given how suitably the coplanar high-eccentricity migration scenario could explain the CWW 89 system, we examine how it might apply to these other systems.

##### • Aligned inner brown dwarf companions:

Findings from both L. Doyle et al. (2025) and T. Ferreira dos Santos et al. (2024) for TOI-2119b and TOI-2533b, respectively, tell a closely-related story to that of the CWW 89 system. These systems share similar values for certain properties with CWW 89Ab with some distinctions that we consider here. Both TOI-2119b and TOI-2533b are massive ( $60\text{--}75 M_J$ ; unlike CWW 89Ab at  $39 M_J$ ) BDs in eccentric orbits ( $e = 0.25\text{--}0.34$ ; similar to CWW 89Ab at  $e = 0.19$ ) between 6.6 and 7.3 days (longer than CWW 89Ab at 5.5 days). As shown in Table 2, TOI-2119b and TOI-2533b are spin-orbit aligned like CWW 89Ab.

What is absent from our current knowledge of these other 2 more-massive BDs is a confirma-

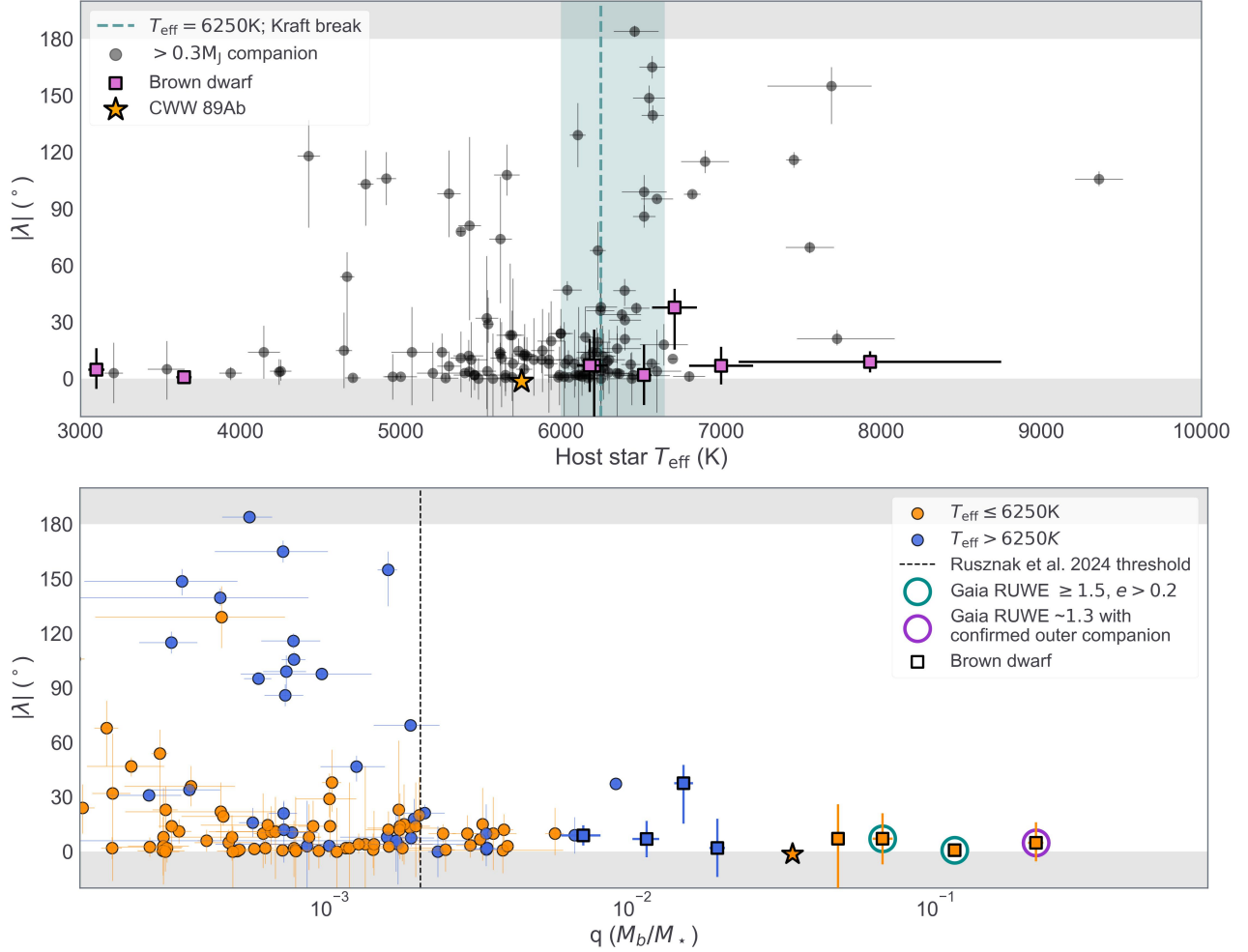


**Figure 4. Top:**  $\lambda$  vs  $T_{\text{eff}}$  for transiting companions  $\gtrsim 0.3 M_J$ . The Kraft Break regime in the vertical shaded region is from A. C. Beyer & R. J. White (2024), with the traditional 6250K threshold denoted by the dashed line. Brown dwarfs are represented by square symbols. CWW 89Ab is the lowest-mass transiting brown dwarf around a sub-Kraft Break star with its  $\lambda$  and  $\psi$  measured. **Bottom:**  $\lambda$  vs  $q$  ( $M_b/M_*$ ) for the same sample in the top panel. We highlight the threshold ( $q = 2 \times 10^{-3}$ ) past which primordial alignment ( $\lambda \approx 0^\circ$ ) dominates the observed distribution (credit to J. Ruzsna et al. 2024). Circled points are systems with inner transiting brown dwarfs and confirmed outer companions (CWW 89 and LP 261-75) or Gaia RUWE values above 1.5. All of the inner brown dwarfs except for the one in LP 261-75 are on eccentric orbits ( $e > 0.18$ ), plausibly following a coplanar HEM scenario. The misaligned giant planet system at  $q \approx 10^{-2}$  is XO-3b discussed in Section 4.2.2. Data in both panels are from Figure 2 of J. Ruzsna et al. (2024).

tion of an outer stellar companion like the detection of CWW 89B. L. Doyle et al. (2025) cite the relatively large re-normalized unweighted error (RUWE, V. Belokurov et al. 2020; Gaia Collaboration et al. 2023) from the Gaia mission of 1.93 for TOI-2119 as an indicator of an unresolved massive companion. An RUWE  $> 1.4$  indicates the strong potential for a binary system (V. Belokurov et al. 2020; D. M. Krolkowski et al. 2021).

Notably, TOI-2119 is an M-dwarf and could join other M-dwarf primary hierarchical triple systems with an inner transiting BD and outer secondary M-dwarf if the high RUWE is proof of an outer

companion. These other hierarchical systems are: LHS 6343 (J. A. Johnson et al. 2011), NLTT 41135 (J. Irwin et al. 2010), NGTS-7 (J. A. G. Jackman et al. 2019), NGTS-28 (B. A. Henderson et al. 2024b), and LP 261-75 (J. M. Irwin et al. 2018; M. Brady et al. 2025). These 5 systems are a part of the total 9 M-dwarf primaries known to host transiting BDs ( $\sim 56\%$ ); the other 4, TOI-2119 included, do not have confirmed outer companions. This emerging trend appears to show BDs that transit M-dwarfs to have a reasonable chance to be part of a hierarchical system with an additional outer M-dwarf. We note that one recent

study by C. Cifuentes et al. (2025) indicates that the M-dwarf multiplicity fraction for separations of 0.01 to  $10^5$  AU ranges from 26% to 42% depending on the confirmation of candidate stellar companions. However, we do robustly not confirm that this is a trend for M-dwarf hosts to transiting BDs here, so the best quantitative evidence for TOI-2119 to host an unresolved M-dwarf companion is its inflated RUWE.

The TOI-2533 system has an RUWE of 1.57, but is an F8 star. With only circumstantial evidence for the existence of an outer companion in the TOI-2119 and TOI-2533 systems via the Gaia RUWE exceeding a value of 1.4, it is not clear if an outer companion would extend the shared characteristics between TOI-2119, TOI-2533, and CWW 89, thus fitting the same coplanar HEM scenario from C. Petrovich (2015). Lastly, if TOI-2119 and TOI-2533 host a secondary M-dwarf companion, we could conclude that the condition in Equation 4 would be satisfied, since we could assume the hypothetical companion orbits exterior to the brown dwarf.

- **Misaligned inner super-Jupiter companion:** XO-3b is a massive  $12 M_J$  planet in a *misaligned* ( $\lambda = 37.8 \pm 3.7^\circ$ ) and eccentric ( $e = 0.28$ ) 3-day orbit (J. N. Winn et al. 2008). This makes XO-3 the singular exception to the observed trend in aligned systems with high mass ratio (Figure 4). J. Rusznak et al. (2024) are the first to point out the RUWE of 1.25 for this system and later confirm the presence of a stellar companion via high-resolution imaging at 90AU. J. Rusznak et al. (2024) argue that this outer stellar companion may have been more of a pivotal factor in the misalignment of XO-3b than the effective temperature of the primary star being above the Kraft Break. This system is the only outlier among other massive companions ( $M_b \gtrsim 10 M_J$ ) with well-determined  $\lambda$  and it is unclear if the outer companion plays a role in this in the same fashion the outer companion to CWW 89A does.

J. Rusznak et al. (2024) argue that the increase in planet-to-star mass ratio correlates with a preference for aligned spin-orbit angles for *single-star* systems. Their conclusions are only valid for single-star systems because these are the objects that they limited their sample to. They provide an explanation for this spin-orbit alignment phenomenon in the circumstellar disks from which these giant planets and brown dwarfs grew. For those systems that experience dynamically disruptive events

early in their formation process, especially in low-mass disks with less mass available to accrete, they may experience a kick that can either or both drive an increase in eccentricity (i.e. high-eccentricity migration) and a misalignment with the plane of the disk and host star, thus depriving the planet of any additional material to grow in mass.

This argument is presented to explain the ubiquity of misaligned sub-Saturn planets around stars above and below the Kraft Break. The opposite of this is seen for brown dwarf-mass and even super-Jupiter mass (i.e.  $\gtrsim 2 M_J$ ) where every system is aligned around hot and cool stars (Figure 4). It is then the Jupiter-mass planets which represent a transitional region in mass where the effects of early-time dynamical excitation affects these planets less strongly than sub-Saturns, but more strongly than super-Jupiters and brown dwarfs. This is a summary of the argument established in J. Rusznak et al. (2024) and it is clear that the transiting brown dwarf population follows this very closely; CWW 89Ab being no exception save for the fact that it is not a single-star system as J. Rusznak et al. (2024) require for their argument to be valid (allowing them to exclude the XO-3 system).

Of the super-Jupiter and brown dwarf systems with measured spin-orbit angles and  $\text{RUWE} \gtrsim 1.25$ , only 1 (XO-3b) in 4 total (CWW 89, TOI-2119, and TOI-2533) is misaligned. As this particular sample continues to grow, we expect it to reveal how the presence of outer companions to transiting brown dwarfs affect spin-orbit alignment. This work and the recent few confirming the aligned orbits of transiting brown dwarfs with the host star’s spin axis all but confirms that the underlying obliquity distribution for these massive companions is consistent with  $\lambda \approx 0^\circ$  as G. Hébrard et al. (2011) establish early in the era of spin-orbit measurements for giant planet and subsequent works by K. Hixenbaugh et al. (2023); T. Gan et al. (2024); S. Giacalone et al. (2024) reinforce.

#### 4.3. Evidence against primordial misalignment

A separate mechanism that describes the realignment of planetary companions is known as “resonance locking” (M. G. Witte & G. J. Savonije 1999; G. J. Savonije 2008). This is when the orbital motion of the companion couples to the host star’s gravity mode ( $g$ -mode) oscillation frequency, resulting in a gradual relative alignment of the companion’s orbit and star’s spin axis. J. J. Zanazzi et al. (2024) simulate a resonance lock scenario using a sunlike star and a  $1 M_J$  companion to explore different timescales over which the companion’s spin-orbit obliquity would realign from misaligned initial condi-



tions (values of  $\psi$  from  $45^\circ$  to  $90^\circ$ ). One important relationship J. J. Zanazzi et al. (2024) show is between the realignment timescale and scaled semi-major axis  $a/R_\star$ , where resonance lock is not possible between a 2.5 Gyr old,  $1 M_\odot$  star (like CWW 89A) and a  $1 M_J$  companion at  $a/R_\star > 10$  within 10 Gyr (Figure 15 in J. J. Zanazzi et al. (2024)). This scenario is for an initial  $\psi = 90^\circ$ .

In our case, the companion almost a factor of 40 more massive, which means that the brown dwarf has an increased tidal potential energy and thus is able to act on the star at larger  $a/R_\star$  than a Jupiter-mass companion. However, even when considering this  $a/R_\star \gtrsim 12$ , the shortest plausible timescale for realignment from  $\psi = 90^\circ$  (when extrapolating from J. J. Zanazzi et al. (2024)) is roughly 9-10 Gyr for CWW 89A, significantly longer than the 2.5 Gyr age of CWW 89. We also highlight the fact that the brown dwarf did not form in its current close orbit, meaning that the couple of its orbital motion to the  $g$ -mode oscillations were likely even weaker for a portion of the system's main sequence lifetime so far. Given this, we find it unlikely that CWW 89A was realigned with the orbital of CWW 89Ab via resonance locking.

## 5. SUMMARY

We report the aligned orbit of the transiting brown dwarf, CWW 89Ab, from our analysis of KPF in-transit RV data measuring the Rossiter-McLaughlin effect. Our main findings are:

- CWW 89Ab has a projected spin-orbit alignment of  $|\lambda| = 1.4 \pm 2.5^\circ$ .
- Given the stellar rotation period and projected stellar rotational velocity (G. Nowak et al. 2017), we find CWW 89Ab has a 3D spin-orbit obliquity of  $\psi = 15.1^{+15.0^\circ}_{-10.1}$  with the posterior distribution peaking at  $\psi_{\text{peak}} = 3.1^\circ$ .
- We confirm trends described in S. Giacalone et al. (2024) and J. Rusznak et al. (2024) that all transiting brown dwarfs ( $M_b \geq 13 M_J$ ) in single- or multi-star systems with measured spin-orbit obliquities are consistent with  $\lambda = 0^\circ$  (aligned) regardless of the primary  $T_{\text{eff}}$ .
- Including CWW 89Ab, total number of transiting BDs with measured  $\lambda$  is 9 and the number with  $\psi$  measured is 3.

We find the trend of massive aligned companions to continue with CWW 89A, plausibly following the orbital evolutionary mechanisms outlined in C. Petrovich

(2015) and J. Rusznak et al. (2024), where a high circumstellar disk mass may have enabled the growth of the brown dwarf into a mass regime where it is resistant to dynamical kicks perpendicular to the disk plane that would have misaligned the brown dwarf's orbit were it closer to or less than the mass of Jupiter. What would then follow is a coplanar high-eccentricity migration induced by the outer companion, assuming the outer companion is coplanar with the brown dwarf. Given the long realignment timescale  $\tau_{\text{CE}} \approx 10$  Gyr between the brown dwarf and primary star and the long circularization timescale  $\tau_{\text{circ}} \gtrsim 7.5$  Gyr relative to the system's age of  $2.8 \pm 0.6$  Gyr, we may conclude that CWW 89Ab formed in an eccentric, aligned orbit. Following the conclusion from T. G. Beatty et al. (2018), if we also assume CWW 89Ab formed via core accretion, then a more complete picture of CWW 89Ab's formation is: core accretion-driven formation and growth in an aligned, eccentric orbit within the circumstellar disk, followed by a coplanar high-eccentricity migration via its outer M-dwarf companion, CWW 89B, inward to its current architectural configuration.

One key missing piece of information is the true separation of CWW 89B from CWW 89A. Future observations with Keck II/NIRC2 could provide constraints on the orbit CWW 89B. Additional high-resolution imaging could also be performed on TOI-2119 and TOI-2533 to search for outer companions and the source of the high RUWE value ( $\gtrsim 1.6$ ) for both of these stars.

## ACKNOWLEDGMENTS

The authors wish to recognize and acknowledge the very significant cultural role and reverence that the summit of Maunakea has always had within the Native Hawaiian community. We are most fortunate to have the opportunity to conduct observations from this mountain.

Some of the data presented herein were obtained at Keck Observatory, which is a private 501(c)3 non-profit organization operated as a scientific partnership among the California Institute of Technology, the University of California, and the National Aeronautics and Space Administration. The Observatory was made possible by the generous financial support of the W. M. Keck Foundation.

This research was carried out, in part, at the Jet Propulsion Laboratory and the California Institute of Technology under a contract with the National Aeronautics and Space Administration and funded through the President's and Director's Research & Development Fund Program.

This research has made use of the NASA Exoplanet Archive, which is operated by the California Institute of Technology, under contract with the National Aeronautics and Space Administration under the Exoplanet Exploration Program.

The research was carried out, in part, at the Jet Propulsion Laboratory, California Institute of Technology, under a contract with the National Aeronautics and

Space Administration (80NM0018D0004) and funded through the President's and Director's Research & Development Fund Program.

TWC is supported by an NSF MPS-Ascend Postdoctoral Fellowship under award 2316566. D.H. acknowledges support from the Alfred P. Sloan Foundation and the National Aeronautics and Space Administration (80NSSC22K0781).

## REFERENCES

- Albrecht, S., Winn, J. N., Johnson, J. A., et al. 2012, *ApJ*, 757, 18, doi: [10.1088/0004-637X/757/1/18](https://doi.org/10.1088/0004-637X/757/1/18)
- Albrecht, S. H., Dawson, R. I., & Winn, J. N. 2022, *PASP*, 134, 082001, doi: [10.1088/1538-3873/ac6c09](https://doi.org/10.1088/1538-3873/ac6c09)
- Beatty, T. G., Morley, C. V., Curtis, J. L., et al. 2018, *AJ*, 156, 168, doi: [10.3847/1538-3881/aad697](https://doi.org/10.3847/1538-3881/aad697)
- Belokurov, V., Penoyre, Z., Oh, S., et al. 2020, *MNRAS*, 496, 1922, doi: [10.1093/mnras/staa1522](https://doi.org/10.1093/mnras/staa1522)
- Beyer, A. C., & White, R. J. 2024, *ApJ*, 973, 28, doi: [10.3847/1538-4357/ad6b0d](https://doi.org/10.3847/1538-4357/ad6b0d)
- Bowler, B. P., Tran, Q. H., Zhang, Z., et al. 2023, *AJ*, 165, 164, doi: [10.3847/1538-3881/acbd34](https://doi.org/10.3847/1538-3881/acbd34)
- Brady, M., Bean, J. L., Stefánsson, G., et al. 2025, *AJ*, 169, 64, doi: [10.3847/1538-3881/ad9c66](https://doi.org/10.3847/1538-3881/ad9c66)
- Bruntt, H., Bedding, T. R., Quirion, P. O., et al. 2010, *MNRAS*, 405, 1907, doi: [10.1111/j.1365-2966.2010.16575.x](https://doi.org/10.1111/j.1365-2966.2010.16575.x)
- Cañas, C. I., Mahadevan, S., Bender, C. F., et al. 2022, *AJ*, 163, 89, doi: [10.3847/1538-3881/ac415f](https://doi.org/10.3847/1538-3881/ac415f)
- Carmichael, T. W., Latham, D. W., & Vanderburg, A. M. 2019, *AJ*, 158, 38, doi: [10.3847/1538-3881/ab245e](https://doi.org/10.3847/1538-3881/ab245e)
- Carmichael, T. W., Irwin, J. M., Murgas, F., et al. 2022, *MNRAS*, 514, 4944, doi: [10.1093/mnras/stac1666](https://doi.org/10.1093/mnras/stac1666)
- Cifuentes, C., Caballero, J. A., González-Payo, J., et al. 2025, *A&A*, 693, A228, doi: [10.1051/0004-6361/202452527](https://doi.org/10.1051/0004-6361/202452527)
- Curtis, J. L., Wolfgang, A., Wright, J. T., Brewer, J. M., & Johnson, J. A. 2013a, *AJ*, 145, 134, doi: [10.1088/0004-6256/145/5/134](https://doi.org/10.1088/0004-6256/145/5/134)
- Curtis, J. L., Wolfgang, A., Wright, J. T., Brewer, J. M., & Johnson, J. A. 2013b, *AJ*, 145, 134, doi: [10.1088/0004-6256/145/5/134](https://doi.org/10.1088/0004-6256/145/5/134)
- David, T. J., Hillenbrand, L. A., Gillen, E., et al. 2019, *ApJ*, 872, 161, doi: [10.3847/1538-4357/aafe09](https://doi.org/10.3847/1538-4357/aafe09)
- Doyle, A. P., Davies, G. R., Smalley, B., Chaplin, W. J., & Elsworth, Y. 2014, *MNRAS*, 444, 3592, doi: [10.1093/mnras/stu1692](https://doi.org/10.1093/mnras/stu1692)
- Doyle, L., Cañas, C. I., Libby-Roberts, J. E., et al. 2025, *MNRAS*, 536, 3745, doi: [10.1093/mnras/stae2819](https://doi.org/10.1093/mnras/stae2819)
- Eastman, J. D., Rodriguez, J. E., Agol, E., et al. 2019, *arXiv e-prints*, arXiv:1907.09480, <https://arxiv.org/abs/1907.09480>
- Espinoza-Retamal, J. I., Jordán, A., Brahm, R., et al. 2024, *arXiv e-prints*, arXiv:2412.08692, doi: [10.48550/arXiv.2412.08692](https://doi.org/10.48550/arXiv.2412.08692)
- Fazio, G. G., Hora, J. L., Allen, L. E., et al. 2004, *ApJS*, 154, 10, doi: [10.1086/422843](https://doi.org/10.1086/422843)
- Ferreira dos Santos, T., Rice, M., Wang, X.-Y., & Wang, S. 2024, *AJ*, 168, 145, doi: [10.3847/1538-3881/ad6b7f](https://doi.org/10.3847/1538-3881/ad6b7f)
- Gaia Collaboration, Vallenari, A., Brown, A. G. A., et al. 2023, *A&A*, 674, A1, doi: [10.1051/0004-6361/202243940](https://doi.org/10.1051/0004-6361/202243940)
- Gan, T., Wang, S. X., Dai, F., et al. 2024, *ApJL*, 969, L24, doi: [10.3847/2041-8213/ad5967](https://doi.org/10.3847/2041-8213/ad5967)
- Giacalone, S., Dai, F., Zanazzi, J. J., et al. 2024, *AJ*, 168, 189, doi: [10.3847/1538-3881/ad785a](https://doi.org/10.3847/1538-3881/ad785a)
- Gibson, S. R., Howard, A. W., Rider, K., et al. 2024a, in *Society of Photo-Optical Instrumentation Engineers (SPIE) Conference Series*, Vol. 13096, Ground-based and Airborne Instrumentation for Astronomy X, ed. J. J. Bryant, K. Motohara, & J. R. D. Vernet, 1309609, doi: [10.1117/12.3017841](https://doi.org/10.1117/12.3017841)
- Gibson, S. R., Howard, A. W., Rider, K., et al. 2024b, in *Society of Photo-Optical Instrumentation Engineers (SPIE) Conference Series*, Vol. 13096, Ground-based and Airborne Instrumentation for Astronomy X, ed. J. J. Bryant, K. Motohara, & J. R. D. Vernet, 1309609, doi: [10.1117/12.3017841](https://doi.org/10.1117/12.3017841)
- Gillen, E., Hillenbrand, L. A., David, T. J., et al. 2017, *ApJ*, 849, 11, doi: [10.3847/1538-4357/aa84b3](https://doi.org/10.3847/1538-4357/aa84b3)
- Hébrard, G., Ehrenreich, D., Bouchy, F., et al. 2011, *A&A*, 527, L11, doi: [10.1051/0004-6361/201016331](https://doi.org/10.1051/0004-6361/201016331)
- Henderson, B. A., Casewell, S. L., Jordán, A., et al. 2024a, *MNRAS*, 533, 2823, doi: [10.1093/mnras/stae1940](https://doi.org/10.1093/mnras/stae1940)
- Henderson, B. A., Casewell, S. L., Goad, M. R., et al. 2024b, *MNRAS*, 530, 318, doi: [10.1093/mnras/stae508](https://doi.org/10.1093/mnras/stae508)

- Hirano, T., Narita, N., Shporer, A., et al. 2011, PASJ, 63, 531, doi: [10.1093/pasj/63.sp2.S531](https://doi.org/10.1093/pasj/63.sp2.S531)
- Hixenbaugh, K., Wang, X.-Y., Rice, M., & Wang, S. 2023, ApJL, 949, L35, doi: [10.3847/2041-8213/acd6f5](https://doi.org/10.3847/2041-8213/acd6f5)
- Irwin, J., Buchhave, L., Berta, Z. K., et al. 2010, ApJ, 718, 1353, doi: [10.1088/0004-637X/718/2/1353](https://doi.org/10.1088/0004-637X/718/2/1353)
- Irwin, J. M., Charbonneau, D., Esquerdo, G. A., et al. 2018, AJ, 156, 140, doi: [10.3847/1538-3881/aad9a3](https://doi.org/10.3847/1538-3881/aad9a3)
- Jackman, J. A. G., Wheatley, P. J., Bayliss, D., et al. 2019, MNRAS, 489, 5146, doi: [10.1093/mnras/stz2496](https://doi.org/10.1093/mnras/stz2496)
- Johns-Krull, C. M., McCullough, P. R., Burke, C. J., et al. 2008, ApJ, 677, 657, doi: [10.1086/528950](https://doi.org/10.1086/528950)
- Johnson, J. A., Apps, K., Gazak, J. Z., et al. 2011, ApJ, 730, 79, doi: [10.1088/0004-637X/730/2/79](https://doi.org/10.1088/0004-637X/730/2/79)
- Knudstrup, E., Albrecht, S. H., Winn, J. N., et al. 2024, A&A, 690, A379, doi: [10.1051/0004-6361/202450627](https://doi.org/10.1051/0004-6361/202450627)
- Kraft, R. P. 1967, ApJ, 150, 551, doi: [10.1086/149359](https://doi.org/10.1086/149359)
- Krolkowski, D. M., Kraus, A. L., & Rizzuto, A. C. 2021, AJ, 162, 110, doi: [10.3847/1538-3881/ac0632](https://doi.org/10.3847/1538-3881/ac0632)
- Larsen, A., Swaby, T. N., Kobulnicky, H. A., et al. 2025, AJ, 169, 246, doi: [10.3847/1538-3881/adbb54](https://doi.org/10.3847/1538-3881/adbb54)
- Leconte, J., Chabrier, G., Baraffe, I., & Levrard, B. 2010, A&A, 516, A64, doi: [10.1051/0004-6361/201014337](https://doi.org/10.1051/0004-6361/201014337)
- Lindgren, L., Hernández, J., Bombrun, A., et al. 2018, A&A, 616, A2, doi: [10.1051/0004-6361/201832727](https://doi.org/10.1051/0004-6361/201832727)
- Masuda, K., & Winn, J. N. 2020, AJ, 159, 81, doi: [10.3847/1538-3881/ab65be](https://doi.org/10.3847/1538-3881/ab65be)
- Nowak, G., Palte, E., Gandolfi, D., et al. 2017, AJ, 153, 131, doi: [10.3847/1538-3881/aa5cb6](https://doi.org/10.3847/1538-3881/aa5cb6)
- Ohta, Y., Taruya, A., & Suto, Y. 2005, ApJ, 622, 1118, doi: [10.1086/428344](https://doi.org/10.1086/428344)
- Petrovich, C. 2015, ApJ, 805, 75, doi: [10.1088/0004-637X/805/1/75](https://doi.org/10.1088/0004-637X/805/1/75)
- Queloz, D., Eggenberger, A., Mayor, M., et al. 2000a, A&A, 359, L13, doi: [10.48550/arXiv.astro-ph/0006213](https://doi.org/10.48550/arXiv.astro-ph/0006213)
- Queloz, D., Eggenberger, A., Mayor, M., et al. 2000b, A&A, 359, L13, doi: [10.48550/arXiv.astro-ph/0006213](https://doi.org/10.48550/arXiv.astro-ph/0006213)
- Rice, M., Wang, S., & Laughlin, G. 2022, ApJL, 926, L17, doi: [10.3847/2041-8213/ac502d](https://doi.org/10.3847/2041-8213/ac502d)
- Ricker, G. R., Winn, J. N., Vanderspek, R., et al. 2015, Journal of Astronomical Telescopes, Instruments, and Systems, 1, 014003, doi: [10.1117/1.JATIS.1.1.014003](https://doi.org/10.1117/1.JATIS.1.1.014003)
- Rusznak, J., Wang, X.-Y., Rice, M., & Wang, S. 2024, arXiv e-prints, arXiv:2412.04438, doi: [10.48550/arXiv.2412.04438](https://doi.org/10.48550/arXiv.2412.04438)
- Saunders, N., Grunblatt, S. K., Chontos, A., et al. 2024, AJ, 168, 81, doi: [10.3847/1538-3881/ad543b](https://doi.org/10.3847/1538-3881/ad543b)
- Savonije, G. J. 2008, in EAS Publications Series, Vol. 29, EAS Publications Series, ed. M. J. Goupil & J. P. Zahn, 91–125, doi: [10.1051/eas:0829003](https://doi.org/10.1051/eas:0829003)
- Schlaflly, E. F., & Finkbeiner, D. P. 2011, ApJ, 737, 103, doi: [10.1088/0004-637X/737/2/103](https://doi.org/10.1088/0004-637X/737/2/103)
- Schmidt, S. P., Schlaufman, K. C., Ding, K., et al. 2023, AJ, 166, 225, doi: [10.3847/1538-3881/ad0135](https://doi.org/10.3847/1538-3881/ad0135)
- Siverd, R. J., Beatty, T. G., Pepper, J., et al. 2012, ApJ, 761, 123, doi: [10.1088/0004-637X/761/2/123](https://doi.org/10.1088/0004-637X/761/2/123)
- Torres, G., Curtis, J. L., Vanderburg, A., Kraus, A. L., & Rizzuto, A. 2018, ApJ, 866, 67, doi: [10.3847/1538-4357/aadca8](https://doi.org/10.3847/1538-4357/aadca8)
- Triaud, A. H. M. J. 2018, in Handbook of Exoplanets, ed. H. J. Deeg & J. A. Belmonte, 2, doi: [10.1007/978-3-319-55333-7\\_2](https://doi.org/10.1007/978-3-319-55333-7_2)
- Triaud, A. H. M. J., Queloz, D., Bouchy, F., et al. 2009, A&A, 506, 377, doi: [10.1051/0004-6361/200911897](https://doi.org/10.1051/0004-6361/200911897)
- Triaud, A. H. M. J., Collier Cameron, A., Queloz, D., et al. 2010, A&A, 524, A25, doi: [10.1051/0004-6361/201014525](https://doi.org/10.1051/0004-6361/201014525)
- Triaud, A. H. M. J., Hebb, L., Anderson, D. R., et al. 2013, A&A, 549, A18, doi: [10.1051/0004-6361/201219643](https://doi.org/10.1051/0004-6361/201219643)
- Vowell, N., Rodriguez, J. E., Quinn, S. N., et al. 2023, AJ, 165, 268, doi: [10.3847/1538-3881/acd197](https://doi.org/10.3847/1538-3881/acd197)
- Vowell, N., Rodriguez, J. E., Latham, D. W., et al. 2025, arXiv e-prints, arXiv:2501.09795, doi: [10.48550/arXiv.2501.09795](https://doi.org/10.48550/arXiv.2501.09795)
- Wang, X.-Y., Rice, M., Wang, S., et al. 2024, ApJL, 973, L21, doi: [10.3847/2041-8213/ad7469](https://doi.org/10.3847/2041-8213/ad7469)
- Wheatley, P. J., West, R. G., Goad, M. R., et al. 2018, MNRAS, 475, 4476, doi: [10.1093/mnras/stx2836](https://doi.org/10.1093/mnras/stx2836)
- Winn, J. N., Fabrycky, D., Albrecht, S., & Johnson, J. A. 2010, ApJL, 718, L145, doi: [10.1088/2041-8205/718/2/L145](https://doi.org/10.1088/2041-8205/718/2/L145)
- Winn, J. N., Noyes, R. W., Holman, M. J., et al. 2005, ApJ, 631, 1215, doi: [10.1086/432571](https://doi.org/10.1086/432571)
- Winn, J. N., Holman, M. J., Torres, G., et al. 2008, ApJ, 683, 1076, doi: [10.1086/589737](https://doi.org/10.1086/589737)
- Witte, M. G., & Savonije, G. J. 1999, A&A, 350, 129, doi: [10.48550/arXiv.astro-ph/9909073](https://doi.org/10.48550/arXiv.astro-ph/9909073)
- Zak, J., Bocchieri, A., Sedaghati, E., et al. 2024, A&A, 686, A147, doi: [10.1051/0004-6361/202349084](https://doi.org/10.1051/0004-6361/202349084)
- Zanazzi, J. J., Dewberry, J., & Chiang, E. 2024, ApJL, 967, L29, doi: [10.3847/2041-8213/ad4644](https://doi.org/10.3847/2041-8213/ad4644)
- Zhang, J., Weiss, L. M., Huber, D., et al. 2025, AJ, 169, 200, doi: [10.3847/1538-3881/ada60a](https://doi.org/10.3847/1538-3881/ada60a)
- Zhou, G., Bakos, G. Á., Bayliss, D., et al. 2019, AJ, 157, 31, doi: [10.3847/1538-3881/aaf1bb](https://doi.org/10.3847/1538-3881/aaf1bb)

**Table 3.** MIST median values and 68% confidence interval for CWW 89A. Here,  $\mathcal{U}[a,b]$  is the uniform prior bounded between  $a$  and  $b$ , and  $\mathcal{G}[a,b]$  is a Gaussian prior of mean  $a$  and width  $b$ .

Parameter	Description	Priors	Values
Stellar Parameters:			
$M_*$ .....	Mass ( $M_\odot$ ).....	-	$1.018^{+0.027}_{-0.026}$
$R_*$ .....	Radius ( $R_\odot$ ).....	-	$1.067 \pm 0.022$
$L_*$ .....	Luminosity ( $L_\odot$ ).....	-	$0.973^{+0.034}_{-0.037}$
$\rho_*$ .....	Density (cgs).....	-	$1.186^{+0.024}_{-0.022}$
$\log g$ ....	Surface gravity (cgs).....	-	$4.391 \pm 0.017$
$T_{\text{eff}}$ ....	Effective temperature (K).....	$\mathcal{G}[5699,200]$	$5553^{+82}_{-86}$
[Fe/H]...	Metallicity (dex).....	$\mathcal{G}[0.12,0.1]$	$0.067 \pm 0.090$
Age.....	Age (Gyr).....	$\mathcal{G}[2.76,0.61]$	$2.52 \pm 0.61$
$A_V$ .....	V-band extinction (mag).....	$\mathcal{U}[0,0.278]$	$0.262^{+0.023}_{-0.045}$
$\sigma_{SED}$ ...	SED photometry error scaling .....	-	$1.13^{+0.47}_{-0.29}$
$\varpi$ .....	Parallax (mas).....	$\mathcal{G}[3.286,0.018]$	$3.282 \pm 0.018$
$d$ .....	Distance (pc).....	-	$304.6 \pm 1.7$
$V_{\text{beta}}$ ...	Gaussian dispersion (m/s).....	$\mathcal{G}[4000,1000]$	$4080^{+1000}_{-990}$
$V_{\text{gamma}}$ ...	Lorentzian dispersion or Differential rotation (m/s)	$\mathcal{U}[1000,1000]$ (fixed)	1000.00
$V_{\text{zeta}}$ ....	Macroturbulence dispersion (m/s).....	-	$3050 \pm 930$
$V_{\text{xi}}$ .....	Microturbulence dispersion (m/s).....	-	$1030^{+880}_{-660}$
Brown dwarf Parameters:			
$P$ .....	Period (days).....	-	$5.2926298^{+0.0000041}_{-0.000086}$
$R_P$ .....	Radius ( $R_J$ ).....	-	$0.963^{+0.037}_{-0.033}$
$M_P$ .....	Mass ( $M_J$ ).....	-	$37.25^{+1.6}_{-0.98}$
$T_C$ .....	Model Time of conjunction <sup>1,2</sup> (TJD <sub>TDB</sub> ).....	-	$2457341.037551^{+0.000095}_{-0.000094}$
$T_0$ .....	Obs time of min proj sep <sup>3,4,5</sup> (BJD <sub>TDB</sub> ).....	-	$2457346.329698^{+0.000094}_{-0.00011}$
$a$ .....	Semi-major axis (AU).....	-	$0.06048^{+0.0013}_{-0.00079}$
$i_0$ .....	Inclination (Degrees).....	-	$88.01^{+0.14}_{-0.13}$
$b$ .....	Transit impact parameter .....	-	$0.429^{+0.013}_{-0.015}$
$e$ .....	Eccentricity .....	-	$0.1892^{+0.0024}_{-0.0029}$
$e \cos \omega_*$ ..	.....	-	$0.1836^{+0.0023}_{-0.0026}$
$e \sin \omega_*$ ..	.....	-	$-0.0450 \pm 0.0032$
$\omega_*$ .....	Arg of periastron (Degrees).....	-	$-13.77^{+0.93}_{-0.89}$
$ \lambda $ .....	Projected Spin-orbit alignment (Degrees).....	-	$1.4^{+2.1}_{-2.5}$
$v \sin i_*$ ..	Projected rotational velocity (m/s).....	-	$4690^{+510}_{-350}$
$T_{\text{eq}}$ .....	Equilibrium temp <sup>6</sup> (K).....	-	$1268 \pm 15$
$K$ .....	RV semi-amplitude (m/s).....	-	$4272^{+18}_{-19}$
$R_P/R_*$ ..	Radius of planet in stellar radii .....	-	$0.09283^{+0.00051}_{-0.00057}$
$a/R_*$ ....	Semi-major axis in stellar radii .....	-	$12.21^{+0.16}_{-0.14}$
$\delta$ .....	$(R_P/R_*)^2$ .....	-	$0.008617^{+0.00010}_{-0.00011}$
$\delta_{\text{Kepler}}$ ..	Transit depth in Kepler (frac).....	-	$0.01076^{+0.00011}_{-0.000100}$
$\tau$ .....	In/egress transit duration (days).....	-	$0.02409^{+0.00090}_{-0.00095}$
$T_{14}$ .....	Total transit duration (days).....	-	$0.15017^{+0.00052}_{-0.00050}$

**Table 3** continued



**Table 3** (*continued*)

Parameter	Description	Priors	Values	
$T_{FWHM}$	FWHM transit duration (days) .....	-	$0.12609^{+0.00067}_{-0.00063}$	
$\rho_P$ .....	Density (cgs) .....	-	$23.4^{+1.6}_{-1.4}$	
$\log g_P$ ...	Surface gravity (cgs) .....	-	$4.764^{+0.019}_{-0.016}$	
$T_P$ .....	Time of Periastron (TJD <sub>TDB</sub> ) .....	-	$2457339.830^{+0.014}_{-0.013}$	
$T_A$ .....	Time of asc node (TJD <sub>TDB</sub> ) .....	-	$2457339.9660 \pm 0.0050$	
$T_D$ .....	Time of desc node (TJD <sub>TDB</sub> ) .....	-	$2457342.7668^{+0.0087}_{-0.0097}$	
$M_P \sin i_0$	Minimum mass ( $M_J$ ) .....	-	$37.23^{+1.6}_{-0.99}$	
$M_P/M_*$	Mass ratio .....	-	$0.03492^{+0.00053}_{-0.00076}$	
Wavelength Parameters:		Kepler	V	
$u_1$ .....	Linear limb-darkening coeff .....	$0.433^{+0.035}_{-0.032}$	$0.502^{+0.052}_{-0.057}$	
$u_2$ .....	Quadratic limb-darkening coeff .....	$0.253 \pm 0.047$	$0.253^{+0.054}_{-0.050}$	
Telescope Parameters:		FIES	KPF	TRES
$\gamma_{\text{rel}}$ .....	Relative RV Offset (m/s) .....	$45642.2^{+9.6}_{-9.0}$	$46716^{+18}_{-230}$	$3481^{+12}_{-13}$
$\sigma_J$ .....	RV Jitter (m/s) .....	$12^{+17}_{-13}$	$5.3^{+1.8}_{-3.5}$	$6.4^{+28}_{-6.4}$
$\sigma_J^2$ .....	RV Jitter Variance .....	$170^{+750}_{-210}$	$27^{+22}_{-25}$	$40^{+1100}_{-590}$
Transit Parameters:		Kepler UT 2015-10-08 (Kepler)		
$\sigma^2$ .....	Added Variance .....	$1.972^{+0.061}_{-0.054} \times 10^{-8}$		
$F_0$ .....	Baseline flux .....	$0.9999990 \pm 0.0000023$		

See Table 3 in [J. D. Eastman et al. \(2019\)](#) for a detailed description of all parameters

<sup>1</sup>Time of conjunction is commonly reported as the “transit time”

<sup>2</sup>BJD<sub>TDB</sub> is the target’s barycentric frame and corrects for light travel time

<sup>3</sup>Time of minimum projected separation is a more correct “transit time”

<sup>4</sup>At the epoch that minimizes the covariance between  $T_C$  and Period

<sup>5</sup>Use this to predict future transit times

<sup>6</sup>Assumes no albedo and perfect redistribution